Published in final edited form as:

Macromolecules. 2018 January 9; 51(1): 173–180. doi:10.1021/acs.macromol.7b01982.

Characterizing the Interface Scaling of High χ Block Copolymers near the Order–Disorder Transition

Daniel F. Sunday[*,†], **Michael J. Maher**[‡], **Adam F. Hannon**[†], **Christopher D. Liman**[†], **Summer Tein**[§], **Gregory Blachut**[§], **Yusuke Asano**[‡], **Christopher J. Ellison**[§,∥], **C. Grant Willson**[‡,§], and **R. Joseph Kline**[†]

[†]Materials Science and Engineering Division, National Institute of Standards and Technology, Gaithersburg, Maryland 20899-1070, United States

[‡]Department of Chemistry, University of Texas at Austin, Austin, Texas 78712, United States

[§]McKetta Department of Chemical Engineering, University of Texas at Austin, Austin, Texas 78712, United States

[∥]Department of Chemical Engineering and Materials Science, University of Minnesota, Minneapolis, Minnesota 55455, United States

Abstract

Advancements in the directed self-assembly of block copolymers (BCPs) have prompted the development of new materials with larger effective interaction parameters (χ_e). This enables BCP systems with phase separation at increasingly small degrees of polymerization (N). Very often these systems reside near the order–disorder transition and fit between the weak and strong segregation limits where the behavior of BCP systems is not as thoroughly understood. Utilizing resonant soft X-ray reflectivity (RSoXR) enables both the BCP pitch (L_0) and interface width (w_M) to be determined simultaneously, through a direct characterization of the composition profile of BCP lamellae oriented parallel to a substrate. A series of high χ_e BCPs with χ_e ranging from ≈0.04 to 0.25 and $\chi_e N$ from 19 to 70 have been investigated. The L_0/w_m ratio serves as an important metric for the feasibility of a material for nanopatterning applications; the results of the RSoXR measurement are used to establish a relationship between χ_e and L_0/w_m. The results of this analysis are correlated with experimentally established limits for the functionality of BCPs in

[*]**Corresponding Author:** daniel.sunday@nist.gov (D.F.S.).

Supporting Information

The Supporting Information is available free of charge on the ACS Publications website at DOI: 10.1021/acs.macromol.7b01982. Figures S1–S4 (PDF)

ORCID

Daniel F. Sunday: 0000-0002-6840-535X
Michael J. Maher: 0000-0003-0577-3726
Adam F. Hannon: 0000-0002-7015-6858
Gregory Blachut: 0000-0002-8539-4840
Christopher J. Ellison: 0000-0002-0393-2941
C. Grant Willson: 0000-0002-2072-3981

Notes

The authors declare no competing financial interest.

nanopatterning applications. These results also provide guidance for the magnitude of χ_e needed to achieve small interface width for samples with sub-10 nm L_0.

Graphical abstract

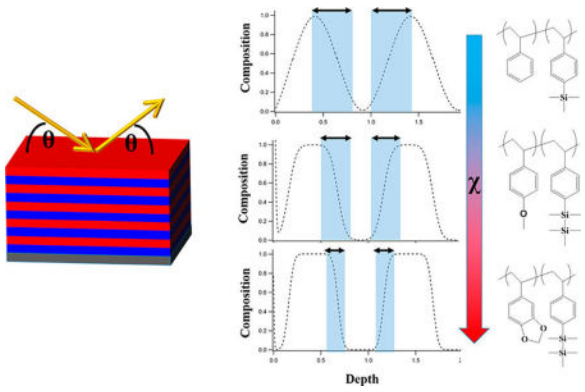

INTRODUCTION

Block copolymers (BCPs) offer intriguing possibilities[1] as templates for patterning membranes,[2–4] metal oxides,[5,6] and other lithographically useful structures.[7–10] The most commonly studied BCPs offer accessibility to feature size and domain period (pitch) length scales between 20 and 100 nm.[11,12] The demonstration of directed self-assembly (DSA) of BCPs as a viable lithographic approach for the semiconductor industry has spurred the development of new BCPs with full pitches below 20 nm and larger inherent etch contrasts.[13–23] Smaller pitches have been achieved by the development of BCPs with large effective Flory–Huggins interaction parameters (χ_e), enabling ordered nanostructures where the degree of polymerization (N) is less than 50 monomer units.[24] Most predictions of the interface or pitch (L_0) scaling assume a sufficiently large N to neglect the effects of chain size.[25–28] As a result, these new high χ_e, low N materials reside in a parameter space that has received relatively little exploration. Most studies on high χ_e BCPs have focused on characterizing L_0, the order–disorder transition (ODT) temperature, and χ_e but have neglected to examine the interface width, which is a potentially limiting factor in the process. Here, we examine the interface width and L_0 scaling of a series of high χ_e silicon-containing BCPs which are currently being explored as candidates for high throughput patterning at sub-20 nm pitch (i.e., sub-10 nm features sizes).[29]

BCP structure, including domain period and morphology, has generally been described by self-consistent field theory (SCFT) where the properties are a function of the volume faction (f_i), statistical segment lengths (b), and the segregation strength $\chi_e N$ (N is the volumetric degree of polymerization calculated according to eq 1 using a common reference volume v_0 = 118 Å^3 where M_n is the number-average molecular mass, ρ is the polymer density, and N_A is Avogadro's constant). SCFT predicts that for an AB diblock copolymer with f_A = 0.5 the ODT occurs at $(\chi_e N)_{ODT} \cong 10.5$.[25,26], This result may not be accurate for materials with a large χ_e and low N, both due to potential deviations from Gaussian chain behavior and due to the impact of composition fluctuations. Several efforts have been made to develop

theories which better reflect the behavior of BCPs under these conditions. For example, Fredrickson–Helfand theory introduces a correction to the ODT prediction which results in an increase in $(\chi_e N)_{ODT}$ for shorter polymer chains to account for fluctuation effects.[30] The renormalized one-loop theory (ROL) was developed in an attempt to model BCP behavior over a wide parameter space. Unlike the earlier theories which depend on N, predictions made by this theory depend on the invariant degree of polymerization, $\bar{N}\left(\bar{N} = Nb^6/v_0^2\right)$. [24,31,32] ROL predicts that composition fluctuations result in an upward shift of $(\chi_e N)_{ODT}$ according to eq 2, which is an empirical relationship derived by analyzing the results of multiple simulation models. The L_0 scaling of lamellar BCPs depends on whether the system is in the weak-segregation-limit regime (WSL, χN near the ODT), where $L_0 \approx N^{1/2}$ or the strong-segregation-limit regime (SSL, $\chi N \gg 10.5$) where $L_0 \approx \chi_e{}^{1/6} N^{2/3}$. A crossover regime where $L_0 \approx N^{4/5}$ has also been observed while transitioning between the WSL and the SSL.[33–36]

$$N = \frac{M_n}{\rho v_0 N_A} \quad (1)$$

$$(\chi_e N)_{ODT} = 10.495 + 41\bar{N}^{-1/3} + 123\bar{N}^{-0.56} \quad (2)$$

In addition to the pitch scaling, there has also been significant investigation into the interface between the two components of a BCP.[37–40] In the WSL the BCP profile is expected to take a sinusoidal shape and show incomplete segregation of the two blocks. In the SSL the two blocks are expected to show a square wave profile with an interface width being inversely proportional to $\chi_e{}^{1/2}$. The interface width between BCP components is typically measured using specular X-ray or neutron reflectivity, which measures the scattering length density (SLD) profile as a function of depth in the film.[40–44] The SLD profile can then be transformed into a composition profile, allowing direct investigation of the composition of a BCP with lamella orientated parallel to the substrate. Historically, neutron reflectivity was the primary tool for these measurements, as the contrast between organic materials for hard X-rays was typically insufficient for accurate structural determination. The drawback to this technique is that it generally requires one of the blocks to be deuterated to enhance the contrast and reduce the incoherent background. This can be synthetically challenging for some materials and can influence the thermodynamics between the blocks.[45] Resonant soft X-ray reflectivity (RSoXR) has emerged recently as a method for enhancing contrast of the native materials based on the type and density of chemical functional groups in the blocks. [46–50] In the soft X-ray region (100–3000 eV) there are absorption edges for the atoms which are the primary constituents of most polymers, carbon (≅285 eV), nitrogen (≅400 eV), and oxygen (≅540 eV). In the vicinity of the absorption edge, the complex refractive index ($n = 1 - (\lambda^2/2\pi)[\rho_R - i\rho_{Im}]$, where λ is the wavelength, ρ_R is the real, or dispersive, component, and ρ_{Im} is the imaginary, or absorptive, component in terms of SLD) will vary sharply. The magnitude of this change depends on the proximity of the beam energy to the absorption edge location (which will shift depending on the exact chemistry) and density of the

functional groups. The measured interface width from this composition profile (w_M) is determined by modeling the interface as an error function, and the width of the error function (σ) is then converted to w_M using eq 3.

$$w_M = \sigma\sqrt{2\pi} \quad (3)$$

Accurate characterization of the interfacial width is important for lithographic materials as it is potentially a limiting factor in the performance of a BCP as an etch mask.[51] Polystyrene-*b*-poly(methyl methacrylate) (PS-*b*-PMMA) is the most commonly explored material for lithographic applications, but it suffers from a number of limitations. Recent results have shown that while the material will form regular patterns down to $L_0 \cong 18$ nm, the pattern will not effectively transfer to the underlying substrate at that length scale.[11] Additionally, PS-*b*-PMMA generally requires enhanced etch selectivity through an additional process such as sequential infiltration synthesis.[52–54] The combination of these two challenges has prompted the development of new BCPs capable of achieving smaller pitches and/or with inherently larger etch contrast. Larger χ_e are generally achieved by increasing the difference in polarity between the two blocks. For example, the addition of a *tert*-butyl group to the PS block of PS-*b*-PMMA enables L_0 as small as 14 nm and a significant shift in the temperature dependence of χ_e.[20] Sub-10 nm domains have been achieved using this approach with poly(cyclohexylethylene)-*b*-PMMA[21] and recently feature sizes as small as 3 nm have been fabricated.[55] There is also some evidence that higher χ_e will lead to a reduction in the line edge roughness (LER).[51] LER values above a tolerable threshold will lead to a deterioration in the electrical properties of the integrated circuit. The degree to which the interface width correlates directly to changes in LER is still unknown.

Silicon-containing BCPs can achieve small pitches and have the advantage of inherently high etch contrast. Block copolymers with poly(dimethylsiloxane) are capable of achieving small feature sizes and good etch transfer to the underlying substrate.[14,17,56,57] In addition to polymers with silicon in the backbone, a series of BCPs with silicon-containing pendant groups have recently been synthesized and studied for DSA applications.[15,58–60] These include (in order of increasing χ_e) PS-*b*-poly(trimethylsilylstyrene) (PS-*b*-PTMSS), PS-*b*-poly-(pentamethyldisylilstyrene) (PS-*b*-PDSS), poly(4-methoxystyrene)-*b*-PTMSS (PMOST-*b*-PTMSS), PMOST-*b*-PDSS, and poly(5-vinyl-1,3-benzodioxole)-*b*-PDSS (PVBD-*b*-PDSS). DSA of PVBD-*b*-PDSS was recently demonstrated with half-pitches of 5 nm on a hybrid chemo/graphoepitaxial template.

In this study we examine the interface width and L_0 scaling for a series of BCPs with χ_e ranging from ≅0.04 (a similar magnitude to that of PS-*b*-PMMA)[61] to ≅0.25 (as determined by SAXS measurements on materials in the disordered phase). The interface widths are characterized using RSoXR to enhance the scattering contrast between the two blocks. Limits on the ratio of w_M/L_0 are explored as a function of $\chi_e N$, which helps explain experimental results demonstrating lower pitch limits on BCP etch transfer.

MATERIALS AND METHODS

Sample Preparation

Block copolymers were prepared via anionic polymerization using the techniques described by Durand et al.[15] Block copolymer solutions (3–5 wt % in methyl isobutyl ketone) were spin coated between 1500 and 3000 rpm to create smooth films on a silicon wafer with native oxide. In this study, it is generally observed that the silicon-containing block prefers to wet the air interface while the other block prefers to wet the substrate surface. The film thicknesses were $(n + 0.5)L_0$ where n is an integer. Films were annealed at 180 °C for 10 min and inspected by optical microscopy to confirm that no topography formed during the annealing process.

RSoXR

RSoXR measurements were performed at the Advanced Light Source (ALS) at the Lawrence Berkeley National Laboratory using beamline 6.3.2. Measurements at the carbon edge (260–300 eV) were conducted using a 600 mm^{-1} grating, a 600 nm Ti filter, and a Burle CEM detector.[62] Measurements at the oxygen edge (520–540 eV) were conducted using a 1200 mm^{-1} grating, a Cr filter, and the Burle CEM detector. The data were fit using the Refl1D program and uncertainties determined using the differential evolution adaptive metropolis (DREAM) algorithm.[63]

RESULTS AND DISCUSSION

The properties of the BCPs examined in this study are outlined in Table 1. For all samples the interaction parameter was previously determined using SAXS measurements in the disordered state.[15,60]

The results of the RSoXR measurements on the PMOST-*b*-PDSS series are shown in Figure 1, where $\chi_e N$ ranged from 32 to 60. The reflectivity curves (Figure 1A) show the classic multilayer signature of a BCP oriented parallel to the substrate. The higher frequency fringes correspond to the total thickness of the film, and the longer spacing between the Bragg peaks corresponds to the L_0 of the polymer. The film prepared from the lowest molecular weight sample (PMOST-*b*-$PDSS_{182}$) has the greatest number of repeating layers in the film (9 full multilayers) and as a result had the sharpest Bragg peaks. The Bragg peak intensity is a function of both the contrast between the layers and the total number of repeating layers. Both the second-order ($q \cong 0.14$ $Å^{-1}$) and third-order ($q \cong 0.24$ $Å^{-1}$) Bragg peaks are clearly visible, showing the slow decay of the Bragg peak intensity. The best fit to this sample results in a w_M = 22.0 [−1.3/+2.0] Å. The samples with larger molecular weights (PMOST-*b*-$PDSS_{251}$, PMOST-*b*-$PDSS_{345}$) show similar behaviors, including both the high frequency fringes and the lower frequency Bragg peaks. As the molecular weight increases, the spacing between the Bragg peaks decreases, consistent with the increase in the BCP domain pitch. The magnitude of the Bragg peaks also decreases because of the reduced number of multilayers in the film. All three samples at different M_n show effectively the same w_M at 22.4 [−1.2/+1.8] Å and 22.8 [−1.3/+1.8] Å for PMOST-*b*-$PDSS_{251}$ and PMOST-*b*-$PDSS_{345}$, respectively. All samples show asymmetry in the uncertainties for w_M, with the uncertainty

in the positive direction being larger than the uncertainty in the negative direction. Shrinking the interface width has a larger impact on the simulated reflectivity than increasing it, and this results in the asymmetry of the uncertainty.

In addition to the results shown in Figure 1, RSoXR measurements were conducted on the remainder of the samples outlined in Table 1. The pitch scaling was explored in order to place the results in context with the behavior of previously investigated BCPs with similar $\chi_e N$. The results of those measurements are shown in the Supporting Information. Figure 2 shows a ln–ln plot of L_0 as a function of N for the three series where multiple molecular masses were examined. All three series show $L_0 \sim N^{3/4}$, a stronger scaling than predicted in either the WSL ($N^{1/2}$) or SSL ($N^{2/3}$). The scaling observed here is closer to previous results which sometimes observed an $N^{4/5}$ scaling in samples with similar $\chi_e N$ (35–80), a regime which is associated with stretched Gaussian coils.[33–36] The origin of the scaling behavior in this region is unclear, but it is shown here to be consistent among samples with a range of χ_e.

For high molecular weight BCPs the interface width is generally small relative to the pitch; for systems near the ODT, the interface region can constitute a significant portion of the BCP. Figure 3 shows the ratio of w_M/L_0 as a function of $\chi_e N$. The PS-*b*-PTMSS series ranges between $\chi_e N = 15$ and 35, and in this region w_M/L_0 can be seen to increase rapidly with decreasing $\chi_e N$, particularly as the ODT is approached (using eq 2 the $(\chi_e N)_{ODT} \approx 13$–15 for most systems investigated in this study). For $\chi_e N > 30$ the w_M/L_0 gradually reduces with increasing $\chi_e N$; this effect is well captured by the PMOST-*b*-PDSS series which spans $40 < \chi_e N < 70$. The two materials with the largest $\chi_e N$ investigated show w_M/L_0 of just above 0.10. There is some spread in the data in this region, which may be caused in part by conformational asymmetry between the two components of the block copolymer which is not captured in this straightforward scaling approach.[64,65] Separating the results into regions above and below $\chi_e N = 35$ allows two different scaling relationships to be extracted from $w_m/L_0 \sim (\chi_e N)^{\omega}$. In the region below $\chi_e N = 35$, $\omega \approx -3/2$; above $\chi_e N = 35$, $\omega \approx -2/3$. Attempting to fit this data with a single power law exponent generally resulted in poor fits to the data below $\chi_e N = 35$; given that the pitch scaling is well-known, this suggests a shift in the scaling of the interface width as the ODT is approached. Experimental results have shown that when $w_m/L_0 \geq 0.27$, etch transfer of a DSA patterned BCP results in large numbers of defects; this limit in relation to the samples investigated in this study is marked in Figure 3. The origin of this behavior can be explained by examining the composition profiles as a function of $\chi_e N$.

The impact of the interface width on the composition profile is captured in Figure 4, which shows the composition profiles for BCP samples with $\chi_e N$ ranging from 19.1 to 72.7. The profiles are normalized by the BCP L_0 to compare materials with a wide range of L_0 on the same graph. PS-*b*-$PTMSS_{392}$ has the lowest $\chi_e N$ value (19.1) and shows both a sinusoidal composition profile and evidence of incomplete phase segregation (i.e., significant regions with composition very close to 1.0 or 0.0 are not observed). PS-*b*-$PTMSS_{478}$ has a slightly larger $\chi_e N$ (23.3) and now shows a narrow region of complete phase segregation near the center of the lamella. As $\chi_e N$ increases, the composition profile rapidly shows signs of increasing phase separation. Increasing $\chi_e N$ to 38.3 (PMOST-*b*-$PDSS_{182}$) shows a clear

transition to the square wave profile associated with the SSL, although the interface still makes up a considerable portion of the profile. PMOST-*b*-PDSS$_{345}$ has the largest $\chi_e N$ examined in this study and results in lamella with a narrow interface. The incomplete phase segregation at $\chi_e N = 19.1$ demonstrates why this represents a lower limit on the patterning ability of BCPs. While the overall structure still results in a lamellar morphology local composition fluctuations are significant enough to result in incomplete phase segregation at many positions along the lamellae. Upon etch transfer these composition fluctuations result in defects. This could be even more problematic near the neutral brush, which likely acts as a compatibilizer and shifts the local $(\chi_e N)_{ODT}$ to a higher value.[12] Both TEM and scattering measurements have suggested that the magnitude of fluctuations increases near the neutral brush.[66,67] It is also possible that this effective patterning limit will shift for BCPs with lower N, where composition fluctuation effects may have a greater impact.

The lower accessible limit of w_M/L_0 for a given L_0 will depend on χ_e and therefore vary depending on the BCP system. This is explored in Figure 5 where w_M/L_0 is shown as a function of L_0. PS-*b*-PTMSS has the lowest χ_e of the BCPs investigated in this study, at $\chi_e \cong 0.04$. As a result, when L_0 decreases, w_M/L_0 increases rapidly, reaching 0.35 at $L_0 = 179$ Å, demonstrating that this system likely has a similar lower accessible pitch limit as PS-*b*-PMMA, which is consistent with the similar magnitude of χ_e for the two materials. As discussed in the previous paragraph, this sample shows incomplete phase segregation. This sample series demonstrates that for a material with this χ_e there is a clear barrier to achieving smaller $L_0 < 100$ Å while maintaining a sufficiently small interface width. As χ_e increases, this limit shifts to progressively lower values. PS-*b*-PDSS has a $\chi_e \cong 0.11$, and w_M/L_0 was found to be 0.17 at $L_0 = 195$ Å, a 40% reduction over the expected value for a PS-*b*-PTMSS sample with identical pitch (w_M/L_0 for PS-*b*-PTMSS with this pitch as extrapolated from the trend). This trend is continued as the BCPs with higher χ_e are examined, shifting the lower limits of w_M/L_0. A rough extrapolation of the data for PMOST-*b*-PDSS suggests that this system could reach a lower patterning limit of $L_0 \approx 90$ Å. While there is insufficient data to determine the lower limit of the PVBD-*b*-PDSS series, experimental results have demonstrated patterning and etch transfer down to $L_0 \approx 100$ Å, suggesting that the lower limits lie at even smaller L_0. Extrapolating from these results also provides an estimate for the magnitude of χ_e which will be needed to obtain $w_M/L_0 < 0.1$ and $L_0 < 100$ Å, which is $\chi_e \approx 0.6–0.7$. This is on the order of the value reported for a recently synthesized polymer, polydihydroxystyrene-*b*-PS,[55] providing additional hope that new BCPs can provide solutions to the patterning needs of next-generation technology nodes.

CONCLUSIONS

Block copolymer lithography requires materials with sufficiently low w_m/L_0 so that the composition fluctuations do not result in defects during etch transfer and the resulting LER does not inhibit electrical performance. By use of RSoXR, the composition profile of a series of high χ_e BCPs was characterized and w_m/L_0 was extracted. This value was scaled as a function of $\chi_e N$, demonstrating a rapid increase as the ODT is approached, and below $\chi_e N = 20$ incomplete phase segregation in the composition profile is observed. This coincides with experimental results showing difficulty in obtaining good etch transfer for a system

with similar w_m/L_0, which provides strong evidence that composition fluctuations limited the etch transfer and that $w_m/L_0 \approx 0.27$ represents an upper limit for effective BCP lithography. w_m/L_0 was also scaled as a function of L_0, demonstrating a shift in the lower accessible L_0 under this limit with increasing χ_e.

Supplementary Material

Refer to Web version on PubMed Central for supplementary material.

Acknowledgments

The Advanced Light Source is supported by the Director, Office of Science, Office of Basic Energy Sciences, of the U.S. Department of Energy under Contract DE-AC02-05CH11231. We thank Eric Gullikson for assistance at BL. 6.3.2. and Paul Kienzle for the work developing the Refl1D software. The authors thank Nissan Chemical Industries, Lam Research, the ASTC, and the National Science Foundation (Grants EECS-1120823 and EEC-1160494) for financial support. M.J.M. thanks National Science Foundation Graduate Research Fellowship (Grant DGE-1110007) for financial support. C.J.E. thanks the Welch Foundation (Grant #F-1709) for partial financial support. G.W. thanks the Rashid Engineering Regents Chair and the Welch Foundation (Grant #F-1830) for partial financial support. Any opinion, findings, and conclusions or recommendations expressed in this material are those of the authors and do not necessarily reflect the views of the National Science Foundation or the sponsors.

References

1. Bates CM, Bates FS. *50th Anniversary Perspective*: Block Polymers—Pure Potential. Macromolecules. 2017; 50(1):3–22.
2. Arges CG, Kambe Y, Suh HS, Ocola LE, Nealey PF. Perpendicularly Aligned, Anion Conducting Nanochannels in Block Copolymer Electrolyte Films. Chem Mater. 2016; 28(5):1377–1389.
3. Kamachi M, Kurihara M, Stille JK. Synthesis of Block Polymers for Desalination Membranes. Preparation of Block Copolymers of 2-Vinylpyridine and Methacrylic Acid or Acrylic Acid. Macromolecules. 1972; 5(2):161–167.
4. Geise GM, Freeman BD, Paul DR. Characterization of a Sulfonated Pentablock Copolymer for Desalination Applications. Polymer. 2010; 51(24):5815–5822.
5. Kamcev J, Germack DS, Nykypanchuk D, Grubbs RB, Nam C-Y, Black CT. Chemically Enhancing Block Copolymers for Block-Selective Synthesis of Self-Assembled Metal Oxide Nanostructures. ACS Nano. 2013; 7(1):339–346. [PubMed: 23252934]
6. Schulze MW, Sinturel C, Hillmyer MA. Poly-(Cyclohexylethylene)- *Block* -Poly(Ethylene Oxide) Block Polymers for Metal Oxide Templating. ACS Macro Lett. 2015; 4(9):1027–1032.
7. Luo M, Epps TH. Directed Block Copolymer Thin Film Self-Assembly: Emerging Trends in Nanopattern Fabrication. Macromolecules. 2013; 46:7567.
8. Kim SO, Solak HH, Stoykovich MP, Ferrier NJ, de Pablo JJ, Nealey PF. Epitaxial Self-Assembly of Block Copolymers on Lithographically Defined Nanopatterned Substrates. Nature. 2003; 424(6947):411–414. [PubMed: 12879065]
9. Ruiz R, Kang H, Detcheverry FA, Dobisz E, Kercher DS, Albrecht TR, de Pablo JJ, Nealey PF. Density Multiplication and Improved Lithography by Directed Block Copolymer Assembly. Science. 2008; 321(5891):936–939. [PubMed: 18703735]
10. Bates CM, Maher MJ, Janes DW, Ellison CJ, Willson CG. Block Copolymer Lithography. Macromolecules. 2014; 47(1):2–12.
11. Wan L, Ruiz R, Gao H, Patel KC, Albrecht TR, Yin J, Kim J, Cao Y, Lin G. The Limits of Lamellae-Forming PS-*b*-PMMA Block Copolymers for Lithography. ACS Nano. 2015; 9(7): 7506–7514. [PubMed: 26046475]
12. Kim E, Choi S, Guo R, Ryu DY, Hawker CJ, Russell TP. Transition Behavior of PS-b-PMMA Films on the Balanced Interfacial Interactions. Polymer. 2010; 51(26):6313–6318.
13. Sweat DP, Kim M, Larson SR, Choi JW, Choo Y, Osuji CO, Gopalan P. Rational Design of a Block Copolymer with a High Interaction Parameter. Macromolecules. 2014; 47(19):6687–6696.

14. Cushen JD, Otsuka I, Bates CM, Halila S, Fort S, Rochas C, Easley JA, Rausch EL, Thio A, Borsali R, Willson CG, Ellison CJ. Oligosaccharide/Silicon-Containing Block Copolymers with 5 Nm Features for Lithographic Applications. ACS Nano. 2012; 6(4):3424–3433. [PubMed: 22456229]
15. Durand WJ, Blachut G, Maher MJ, Sirard S, Tein S, Carlson MC, Asano Y, Zhou SX, Lane AP, Bates CM, Ellison CJ, Willson CG. Design of High-χ Block Copolymers for Lithography. J Polym Sci, Part A: Polym Chem. 2015; 53(2):344–352.
16. Maher MJ, Mori K, Sirard SM, Dinhobl AM, Bates CM, Gurer E, Blachut G, Lane AP, Durand WJ, Carlson MC, Strahan JR, Ellison CJ, Willson CG. Pattern Transfer of Sub-10 Nm Features via Tin-Containing Block Copolymers. ACS Macro Lett. 2016; 5(3):391–395.
17. Luo Y, Montarnal D, Kim S, Shi W, Barteau KP, Pester CW, Hustad PD, Christianson MD, Fredrickson GH, Kramer EJ, Hawker CJ. Poly(Dimethylsiloxane-*b*-Methyl Methacrylate): A Promising Candidate for Sub-10 Nm Patterning. Macromolecules. 2015; 48(11):3422–3430.
18. Shi W, Tateishi Y, Li W, Hawker CJ, Fredrickson GH, Kramer EJ. Producing Small Domain Features Using Miktoarm Block Copolymers with Large Interaction Parameters. ACS Macro Lett. 2015; 4(11):1287–1292.
19. Sinturel C, Bates FS, Hillmyer MA. High X–Low *N* Block Polymers: How Far Can We Go? ACS Macro Lett. 2015; 4(9):1044–1050.
20. Kennemur JG, Hillmyer MA, Bates FS. Synthesis, Thermodynamics, and Dynamics of Poly(4-Tert-Butylstyrene- b -Methyl Methacrylate). Macromolecules. 2012; 45(17):7228–7236.
21. Kennemur JG, Yao L, Bates FS, Hillmyer MA. Sub-5 Nm Domains in Ordered Poly(Cyclohexylethylene)- *Block* -Poly-(Methyl Methacrylate) Block Polymers for Lithography. Macromolecules. 2014; 47(4):1411–1418.
22. Vora A, Wojtecki RJ, Schmidt K, Chunder A, Cheng JY, Nelson A, Sanders DP. Development of Polycarbonate-Containing Block Copolymers for Thin Film Self-Assembly Applications. Polym Chem. 2016; 7(4):940–950.
23. Yang G-W, Wu G-P, Chen X, Xiong S, Arges CG, Ji S, Nealey PF, Lu X-B, Darensbourg DJ, Xu Z-K. Directed Self-Assembly of Polystyrene-*b*-Poly(Propylene Carbonate) on Chemical Patterns via Thermal Annealing for Next Generation Lithography. Nano Lett. 2017; 17(2):1233–1239. [PubMed: 28068100]
24. Gillard TM, Medapuram P, Morse DC, Bates FS. Fluctuations, Phase Transitions, and Latent Heat in Short Diblock Copolymers: Comparison of Experiment, Simulation, and Theory. Macromolecules. 2015; 48(8):2801–2811.
25. Bates FS, Fredrickson GH. Block Copolymer Thermodynamics: Theory and Experiment. Annu Rev Phys Chem. 1990; 41(1):525–557. [PubMed: 20462355]
26. Leibler L. Theory of Microphase Separation in Block Copolymers. Macromolecules. 1980; 13(6): 1602–1617.
27. Broseta D, Fredrickson GH, Helfand E, Leibler L. Molecular Weight and Polydispersity Effects at Polymer-Polymer Interfaces. Macromolecules. 1990; 23(1):132–139.
28. Helfand E, Tagami Y. Theory of the Interface between Immiscible Polymers. II. J Chem Phys. 1972; 56(7):3592.
29. Blachut G, Sirard SM, Maher MJ, Asano Y, Someya Y, Lane AP, Durand WJ, Bates CM, Dinhobl AM, Gronheid R, Hymes D, Ellison CJ, Willson CG. A Hybrid Chemo-/Grapho-Epitaxial Alignment Strategy for Defect Reduction in Sub-10 Nm Directed Self-Assembly of Silicon-Containing Block Copolymers. Chem Mater. 2016; 28(24):8951–8961.
30. Fredrickson GH, Helfand E. Fluctuation Effects in the Theory of Microphase Separation in Block Copolymers. J Chem Phys. 1987; 87(1):697.
31. Medapuram P, Glaser J, Morse DC. Universal Phenomenology of Symmetric Diblock Copolymers near the Order–Disorder Transition. Macromolecules. 2015; 48(3):819–839.
32. Glaser J, Qin J, Medapuram P, Müller M, Morse DC. Test of a Scaling Hypothesis for the Structure Factor of Disordered Diblock Copolymer Melts. Soft Matter. 2012; 8(44):11310.
33. Sivaniah E, Hayashi Y, Matsubara S, Kiyono S, Hashimoto T, Fukunaga K, Kramer EJ, Mates T. Symmetric Diblock Copolymer Thin Films on Rough Substrates. Kinetics and Structure Formation in Pure Block Copolymer Thin Films. Macromolecules. 2005; 38(5):1837–1849.

34. Almdal K, Rosedale JH, Bates FS, Wignall GD, Fredrickson GH. Gaussian-to Stretched-Coil Transition in Block Copolymer Melts. Phys Rev Lett. 1990; 65(9):1112. [PubMed: 10043108]
35. Hadziioannou G, Skoulios A. Molecular Weight Dependence of Lamellar Structure in Styrene Isoprene Two-and Three-Block Copolymers. Macromolecules. 1982; 15(2):258–262.
36. Papadakis CM, Almdal K, Mortensen K, Posselt D. Identification of an Intermediate-Segregation Regime in a Diblock Copolymer System. EPL Europhys Lett. 1996; 36(4):289.
37. Foster MD, Sikka M, Singh N, Bates FS, Satija SK, Majkrzak CF. Structure of Symmetric Polyolefin Block Copolymer Thin Films. J Chem Phys. 1992; 96(11):96.
38. Winey KI, Thomas EL, Fetters LJ. Ordered Morphologies in Binary Blends of Diblock Copolymer and Homopolymer and Characterization of Their Intermaterial Dividing Surfaces. J Chem Phys. 1991; 95:9367.
39. Scherble J, Stark B, Stühn B, Kressler J, Budde H, Höring S, Schubert DW, Simon P, Stamm M. Comparison of Interfacial Width of Block Copolymers of d_8 -Poly(Methyl Methacrylate) with Various Poly(n -Alkyl Methacrylate)s and the Respective Homopolymer Pairs as Measured by Neutron Reflection. Macromolecules. 1999; 32(6):1859–1864.
40. Russell TP, Anastasiadis SH, Menelle A, Felcher GP, Satija SK. Segment Density Distribution of Symmetric Diblock Copolymers at the Interface between Two Homopolymers as Revealed by Neutron Reflectivity. Macromolecules. 1991; 24(7):1575–1582.
41. Russell TP. On the Reflectivity of Polymers: Neutrons and X-Rays. Phys B. 1996; 221(1):267–283.
42. Russell TP, Menelle A, Hamilton WA, Smith GS, Satija SK, Majkrzak CF. Width of Homopolymer Interfaces in the Presence of Symmetric Diblock Copolymers. Macromolecules. 1991; 24(20): 5721–5726.
43. Anastasiadis SH, Russell TP, Satija SK, Majkrzak CF. The Morphology of Symmetric Diblock Copolymers as Revealed by Neutron Reflectivity. J Chem Phys. 1990; 92(9):92.
44. Stamm M. Investigation of the Interface between Polymers: A Comparison of Scattering and Reflectivity Techniques. J Appl Crystallogr. 1991; 24(5):651–658.
45. Harton SE, Stevie FA, Zhu Z, Ade H. Changes in Thermodynamic Interactions at Highly Immiscible Polymer/Polymer Interfaces Due to Deuterium Labeling. J Phys Chem B. 2006; 110(22):10602–10605. [PubMed: 16771304]
46. Wang C, Araki T, Ade H. Soft X-Ray Resonant Reflectivity of Low-Z Material Thin Films. Appl Phys Lett. 2005; 87(21):87.
47. Ade H, Wang C, Garcia A, Yan H, Sohn KE, Hexemer A, Bazan GC, Nguyen T-Q, Kramer EJ. Characterization of Multicomponent Polymer Trilayers with Resonant Soft X-Ray Reflectivity. J Polym Sci, Part B: Polym Phys. 2009; 47(13):1291–1299.
48. Yan H, Wang C, Garcia A, Swaraj S, Gu Z, McNeill CR, Schuettfort T, Sohn KE, Kramer EJ, Bazan GC, Nguyen T-Q, Ade H. Interfaces in Organic Devices Studied with Resonant Soft X-Ray Reflectivity. J Appl Phys. 2011; 110(10):110.
49. Mezger M, Ocko BM, Reichert H, Deutsch M. Surface Layering and Melting in an Ionic Liquid Studied by Resonant Soft X-Ray Reflectivity. Proc Natl Acad Sci U S A. 2013; 110(10):3733–3737. [PubMed: 23431181]
50. Sunday DF, Kline RJ. Reducing Block Copolymer Interfacial Widths through Polymer Additives. Macromolecules. 2015; 48(3):679–686.
51. Kim JM, Hur YH, Jeong JW, Nam TW, Lee JH, Jeon K, Kim Y, Jung YS. Block Copolymer with an Extremely High Block-to-Block Interaction for a Significant Reduction of Line-Edge Fluctuations in Self-Assembled Patterns. Chem Mater. 2016; 28:5680.
52. Peng Q, Tseng Y-C, Darling SB, Elam JW. A Route to Nanoscopic Materials *via* Sequential Infiltration Synthesis on Block Copolymer Templates. ACS Nano. 2011; 5(6):4600–4606. [PubMed: 21545142]
53. Tseng Y-C, Peng Q, Ocola LE, Elam JW, Darling SB. Enhanced Block Copolymer Lithography Using Sequential Infiltration Synthesis. J Phys Chem C. 2011; 115(36):17725–17729.
54. Tseng Y-C, Peng Q, Ocola LE, Czaplewski DA, Elam JW, Darling SB. Etch Properties of Resists Modified by Sequential Infiltration Synthesis. J Vac Sci Technol, B: Nanotechnol Microelectron: Mater, Process, Meas, Phenom. 2011; 29(6):06FG01.

55. Kwak J, Mishra AK, Lee J, Lee KS, Choi C, Maiti S, Kim M, Kim JK. Fabrication of Sub-3 Nm Feature Size Based on Block Copolymer Self-Assembly for Next-Generation Nanolithography. Macromolecules. 2017; 50(17):6813–6818.
56. Son JG, Hannon AF, Gotrik KW, Alexander-Katz A, Ross CA. Hierarchical Nanostructures by Sequential Self-Assembly of Styrene-Dimethylsiloxane Block Copolymers of Different Periods. Adv Mater. 2011; 23(5):634–639. [PubMed: 21274911]
57. Rodwogin MD, Spanjers CS, Leighton C, Hillmyer MA. Polylactide–Poly(Dimethylsiloxane)–Polylactide Triblock Copolymers as Multifunctional Materials for Nanolithographic Applications. ACS Nano. 2010; 4(2):725–732. [PubMed: 20112923]
58. Maher MJ, Rettner CT, Bates CM, Blachut G, Carlson MC, Durand WJ, Ellison CJ, Sanders DP, Cheng JY, Willson CG. Directed Self-Assembly of Silicon-Containing Block Copolymer Thin Films. ACS Appl Mater Interfaces. 2015; 7(5):3323–3328. [PubMed: 25594107]
59. Cushen J, Wan L, Blachut G, Maher MJ, Albrecht TR, Ellison CJ, Willson CG, Ruiz R. Double-Patterned Sidewall Directed Self-Assembly and Pattern Transfer of Sub-10 Nm PTMSS-*b*-PMOST. ACS Appl Mater Interfaces. 2015; 7(24):13476–13483. [PubMed: 26004013]
60. Lane AP, Yang X, Maher MJ, Blachut G, Asano Y, Someya Y, Mallavarapu A, Sirard SM, Ellison CJ, Willson CG. Directed Self-Assembly and Pattern Transfer of Five Nanometer Block Copolymer Lamellae. ACS Nano. 2017; 11:7656. [PubMed: 28700207]
61. Zhao Y, Sivaniah E, Hashimoto T. SAXS Analysis of the Order- Disorder Transition and the Interaction Parameter of Polystyrene-Block-Poly (Methyl Methacrylate). Macromolecules. 2008; 41(24):9948–9951.
62. Certain commercial equipment, instruments, or materials are identified in this paper in order to specify the experimental procedure adequately. Such identification is not intended to imply recommendation or endorsement by the National Institute of Standards and Technology, nor is it intended to imply that the materials or equipment identified are necessarily the best available for the purpose.
63. Vrugt JA, Ter Braak CJF. $\text{DREAM}_{(D)}$: An Adaptive Markov Chain Monte Carlo Simulation Algorithm to Solve Discrete, Noncontinuous, and Combinatorial Posterior Parameter Estimation Problems. Hydrol Earth Syst Sci. 2011; 15(12):3701–3713.
64. Gehlsen MD, Bates FS. Conformational Asymmetry in Poly (Vinylcyclohexane) Containing Diblock Copolymers. Macromolecules. 1994; 27(13):3611–3618.
65. Bates FS, Schulz MF, Khandpur AK, Förster S, Rosedale JH, Almdal K, Mortensen K. Fluctuations, Conformational Asymmetry and Block Copolymer Phase Behaviour. Faraday Discuss. 1994; 98:7–18.
66. Segal-Peretz T, Ren J, Xiong S, Khaira G, Bowen A, Ocola LE, Divan R, Doxastakis M, Ferrier NJ, de Pablo J, Nealey PF. Quantitative Three-Dimensional Characterization of Block Copolymer Directed Self-Assembly on Combined Chemical and Topographical Prepatterned Templates. ACS Nano. 2017; 11:1307. [PubMed: 28005329]
67. Khaira G, Doxastakis M, Bowen A, Ren J, Suh HS, Segal-Peretz T, Chen X, Zhou C, Hannon AF, Ferrier NJ, Vishwanath V, Sunday DF, Gronheid R, Kline RJ, de Pablo JJ, Nealey PF. Derivation of Multiple Covarying Material and Process Parameters Using Physics-Based Modeling of X-Ray Data. Macromolecules. 2017; 50(19):7783–7793.

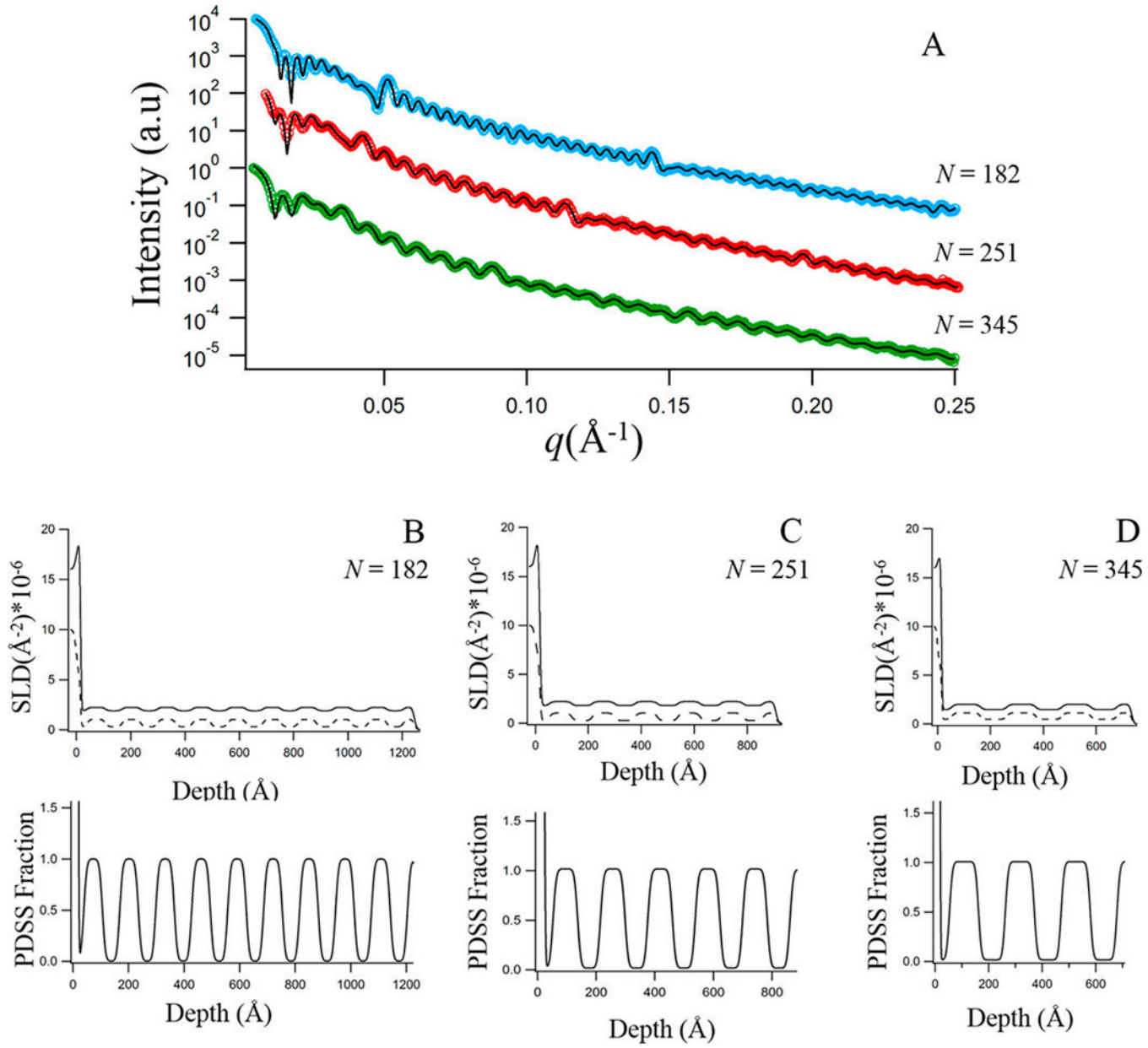

Figure 1.

Experimental (colored ○) and simulated fits (solid lines) for PMOST-*b*-PDSS for $N = 182$, 251, and 345. Measurements were collected at either 282 or 282.5 eV. The corresponding SLD (solid lines indicate ρ_R, dashed lines indicate ρ_{Im}) and SLD/composition plots are shown in B ($N = 182$), C ($N = 251$), and D ($N = 345$). Composition plots exceed 1 at the SiO_2 layer.

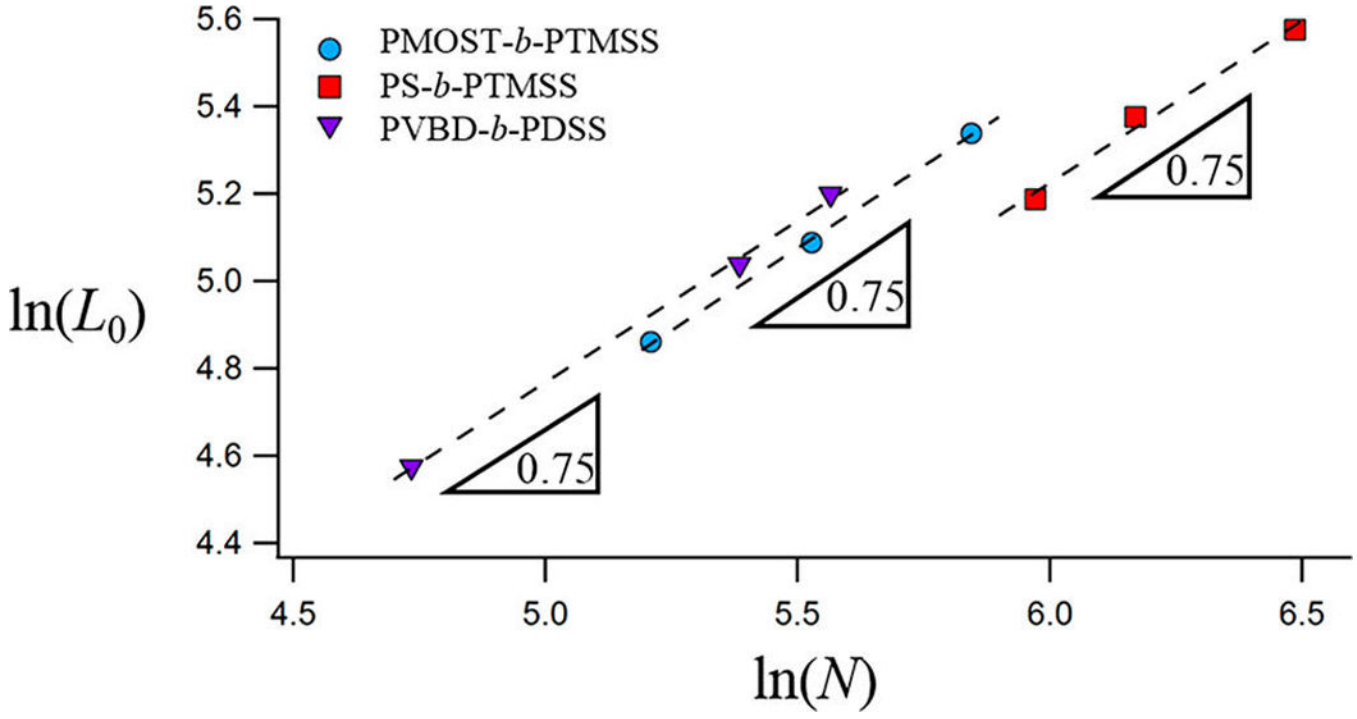

Figure 2.
Plot showing ln(L_0) as a function of ln(N); all sample sets show slopes of ≈0.75.

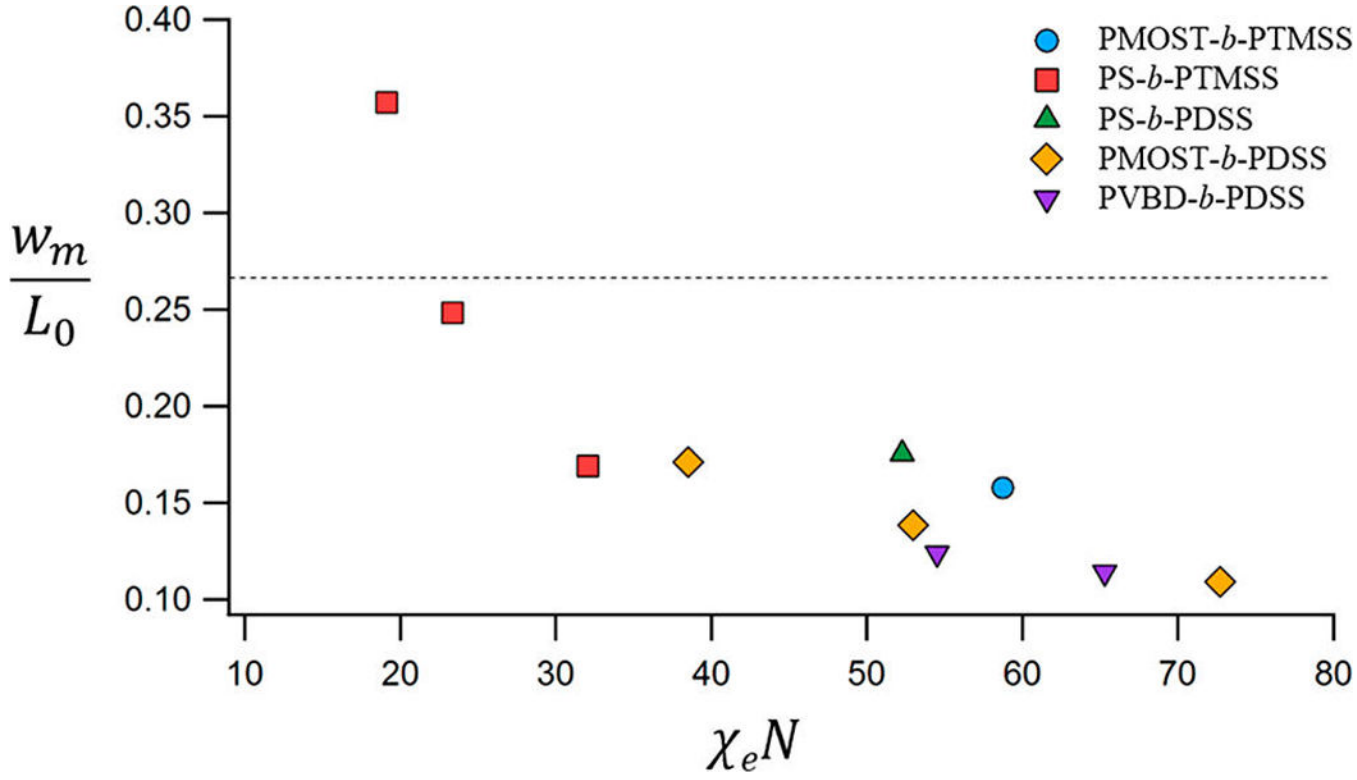

Figure 3.

Ratio of w_m/L_0 as a function of $\chi_e N$. From these results a scaling relationship can be extracted, $w_m/L_0 \sim (\chi_e N)^{\omega}$. For $\chi_e N < 35$ $\omega \approx -3/2$, and for $\chi_e N > 35$ $\omega \approx -2/3$. For systems with w_m/L_0 above 0.27 (dashed line) experimental results have shown a loss of alignment upon etching one of the components in the polymer.[11]

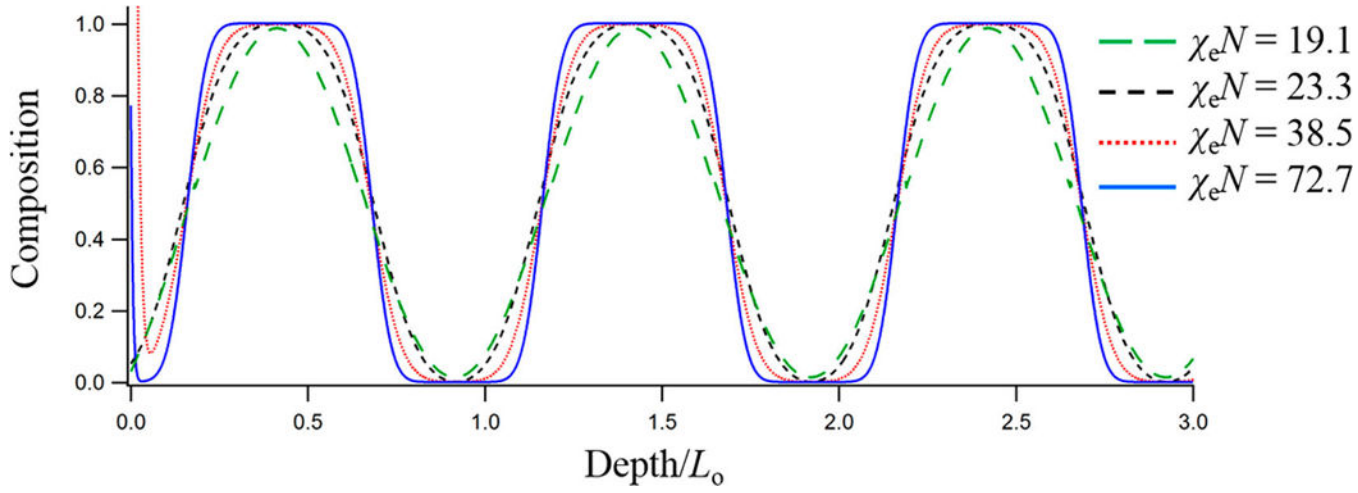

Figure 4.

Composition profile for BCPs with $\chi_e N = 191$ (PS-*b*-$PTMSS_{392}$), $\chi_e N = 23.3$ (PS-*b*-$PTMSS_{478}$), $\chi_e N = 38.5$ (PMOST-*b*-$PDSS_{182}$), and $\chi_e N = 72.7$ (PS-*b*-$PTMSS_{345}$). The profiles are normalized by L_0 in order to compare the shape of the composition profile for the BCPs on the same scale. They are also shifted in order to account for the small differences in the SiO_2 thickness in the model so that the minima and maxima of the profiles are centered at the same location.

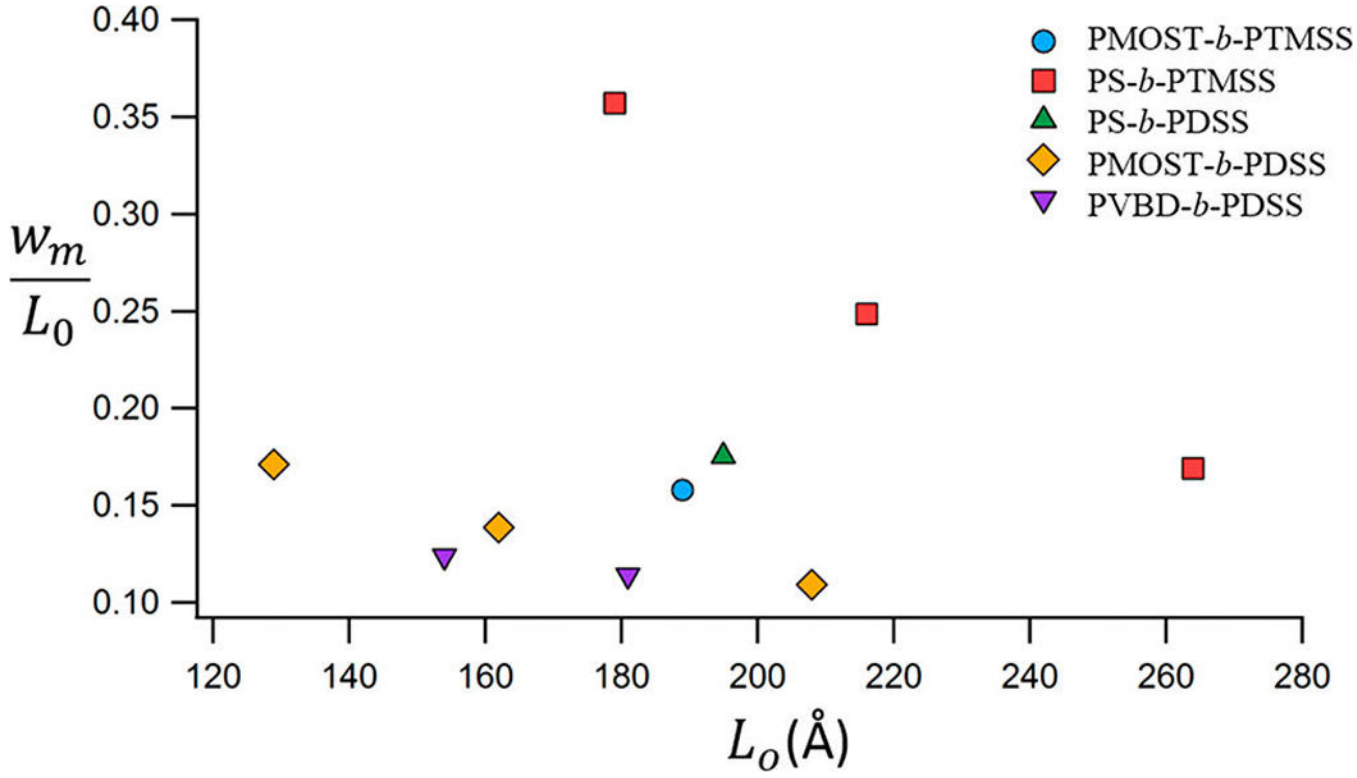

Figure 5.
w_M/L_0 as a function of L_0 for all BCP samples.

Table 1

Sample Parameters, χ_e, w_M, and L_0 from RSoXR Measurements

sample name	M_n [kg/mol] (A block)	M_n [kg/mol] (B block)	N^a	χ_e(SAXS)^b at 180 °C	$\chi_e N$ (SAXS)	w_M (Å)	L_0 (Å)
PS-*b*-PTMSS$_{392}$	14.0	14.4	392	0.047	19.1	63.9 [−3.9/+9.8]	179 ± 2.7
PS-*b*-PTMSS$_{478}$	16.7	17.4	478	0.047	23.3	53.6 [1.3/+5.3]	216 ± 2.6
PS-*b*-PTMSS$_{656}$	23.7	23.2	656	0.047	32.0	44.6 [−1.0/+6.9]	264 ± 2.7
PS-*b*-PDSS$_{426}$	15.0	14.7	426	0.112	52.3	34.2 [−1.4/+3.8]	195 ± 2.2
PMOST-*b*-PTMSS$_{369}$	14.4	13.0	369	0.135	58.7	29.8 [−0.8/+1.3]	189 ± 2.3
PMOST-*b*-PDSS$_{182}$	7.4	5.9	182	0.195	38.5	22.0 [−1.3/+2.0]	129 ± 2.3
PMOST-*b*-PDSS$_{251}$	9.7	8.5	251	0.195	53.0	22.4 [−1.2/+1.8]	162 ± 2.4
PMOST-*b*-PDSS$_{345}$	12.3	12.5	345	0.195	72.7	22.8 [−1.3/+1.8]	208 ± 2.4
PVBD-*b*-PDSS$_{218}$	8.9	7.4	218	0.25	65.3	19.0 [−1.1/+1.9]	154 ± 2.1
PVBD-*b*-PDSS$_{261}$	11.0	8.6	261	0.25	54.5	20.6 [−1.6/+2.6]	181 ± 2.3

[a] N was calculated using eq 1, densities were experimentally determined previously,[15] and a common reference volume of v_0 = 118 Å^3 was used for all samples.

[b] All values were calculated at 180 °C, based on SAXS measurements of disordered materials.[15]